Biomaterials Science

ROYAL SOCIETY OF CHEMISTRY

PAPER

View Article Online
View Journal | View Issue

Cite this: *Biomater. Sci.*, 2023, **11**, 6823

Prodrug-loaded semiconducting polymer hydrogels for deep-tissue sono-immunotherapy of orthotopic glioblastoma†

Liyun Zhu,‡[a] Xing Wang,‡[a] Mengbin Ding,[a] Ningyue Yu,[a] Yijing Zhang,[a] Hongwei Wu, *[a] Qin Zhang, *[c] Jiansheng Liu*[b] and Jingchao Li *[a]

Although immunotherapy has achieved great success in the treatment of a variety of tumors, its efficacy for glioblastoma (GBM) is still limited. Both the immunosuppressive tumor microenvironment (TME) and poor penetration of immunotherapeutic agents into tumors contributed to the poor anti-glioma immunity. Herein, we develop an injectable prodrug-loaded hydrogel delivery system with sono-activatable properties for sonodynamic therapy (SDT)-triggered immunomodulation for GBM treatment. The prodrug alginate hydrogels (APN), which contain semiconducting polymer nanoparticles (SPNs) and the NLG919 prodrug linked by singlet oxygen ($^1O_2$)-cleavable linkers, are *in situ* formed *via* coordination of alginate solution with Ca^{2+} in the TME. SPNs serve as sonosensitizers to produce $^1O_2$ upon ultrasound (US) irradiation for SDT. The generated $^1O_2$ not only induce immunogenic cell death, but also break $^1O_2$-cleavable linkers to precisely activate the NLG919 prodrug. Antitumor immunity is significantly amplified due to the reversal of immunosuppression mediated by indolamine 2,3-dioxygenase-dependent tryptophan metabolism. This smart prodrug hydrogel platform potently inhibits tumor growth in orthotopic glioma-bearing mice. Collectively, this work provides a sono-activatable hydrogel platform for precise sono-immunotherapy against GBM.

Received 8th April 2023,
Accepted 10th August 2023

DOI: 10.1039/d3bm00585b

rsc.li/biomaterials-science

1. Introduction

Glioblastoma (GBM) is the most aggressive and lethal primary brain tumor.[1–3] The invasive nature of glioblastoma cells makes it difficult to completely remove them through surgery, leading to a high rate of recurrence. Additionally, GBM cells are resistant to traditional chemotherapy and radiotherapy, further complicating treatment options.[4,5] As a result, GBM patients have a poor prognosis, with a median survival time of only 15 months and a five year survival rate less than 5%.[6] Therefore, there is still an urgent need to explore novel approaches for combating this malignancy.

Immunotherapy, which uses checkpoint inhibitors, cytokines, antibodies and/or engineered T cells to mobilize the immune system for attacking cancer cells, has become a revolutionary modality in cancer treatment.[7–10] This therapeutic modality shows unique advantages in eliminating primary tumors, inhibiting tumor metastasis and preventing elapse. Several preclinical and clinical trials have been performed to assess the efficacy of immunotherapy against glioma.[11] Nevertheless, the antitumor activity of current immunotherapies against GBM was far from satisfactory, which could be ascribed to the "cold" immunosuppressive tumor microenvironment (TME) of GBM and poor penetration of immunotherapeutic agents into tumors.[12–17] Glioma cells express increased amounts of immunosuppressive molecules, including programmed cell death 1 ligand (PD-L1) and indolamine 2,3-dioxygenase (IDO), which greatly attenuate the antigen-presenting effect.[18,19] Besides, the level of regulatory T cells (T_{reg}) is significantly increased in the GBM microenvironment, leading to the depletion of effector T cells.[20–22] Furthermore, the presence of the blood–brain barrier greatly restricts the penetration of immunotherapeutic drugs and the infiltration of immune cells into tumor tissues, undermining immunotherapy efficacy against GBM.[23,24]

Modulation of the immunosuppressive TME is highly desired to enhance antitumor immune responses for GBM

[a]*State Key Laboratory for Modification of Chemical Fibers and Polymer Materials, Shanghai Engineering Research Center of Nano-Biomaterials and Regenerative Medicine, College of Chemistry, Chemical Engineering and Biotechnology, Donghua University, Shanghai 201620, China. E-mail: wuhongwei@dhu.edu.cn, jcli@dhu.edu.cn*

[b]*Department of Neurology, Zhongshan-Xuhui Hospital, Fudan University, Shanghai 200032, China. E-mail: drjianshengliu84@gmail.com*

[c]*Institute of Translational Medicine, Shanghai University, Shanghai 200444, China. E-mail: sabrina_1985@shu.edu.cn*

†Electronic supplementary information (ESI) available. See DOI: https://doi.org/10.1039/d3bm00585b

‡These authors contributed equally to this work.

treatment.[25] Traditional therapies including radiotherapy and chemotherapy could improve the immunogenicity of tumors *via* inducing immunogenic cell death (ICD) of dying tumor cells.[26–29] Therefore, a combination of ICD induction with immunotherapy is a promising strategy to treat GBM. For example, local delivery of an ICD inducer doxorubicin and a Toll-like receptor (TLR)-9 agonist CpG into tumors elicited antitumor $CD8^+$ T cell responses and reduced the infiltration of M2-like tumor-associated macrophages and myeloid-derived suppressor cells in the brain TME.[30] The rapid development of biomaterials and nanobiotechnology provides more efficient alternatives to achieve this strategy.[31] A tumor-homing immune nanoregulator was constructed by co-entrapping chemotherapeutic mitoxantrone as an ICD inducer and small interfering RNAs that target IDO in zinc 2-methylimidazole-based nanocarriers and then cloaking with a glioma-associated macrophage membrane.[32] Such a nanoregulator was co-delivered with CXC chemokine ligand 10 in a self-fabricating oligopeptide hydrogel to inhibit GBM relapse post-resection. Compared to the conventional ICD inducer, a nanoinducer composed of disulfide bond-incorporated organosilica nanoparticles, curcumin, and iron oxide nanoparticles demonstrates a notable enhancement in ICD-inducing activity and tumor cell specificity.[33] However, ICD induced by organic and/or inorganic compounds still lacks sufficient efficiency and specificity.

Sonodynamic therapy (SDT) is a novel modality of ultrasound (US) therapy in which sonosensitizers are used to generate singlet oxygen ($^1O_2$) for killing neoplastic cells.[34] As a non-invasive external stimulus, US has the advantages of high selectivity and specificity.[35,36] Beyond this, SDT has shown particular advantages in the treatment of deep-seated tumors due to the strong penetrating ability of US.[37,38] Significantly, ICD can be effectively induced by SDT to trigger robust antitumor immune responses, termed sonodynamic immunotherapy.[35,39,40]

A key bottleneck of current cancer immunotherapy is immune-related adverse events (irAEs) due to uncontrolled modulation of the immune system.[41,42] Prodrug-based nanomedicines have been explored as a means to address this challenge.[43] Prodrugs are designed by chemically modifying small molecules, peptides, or antibodies to enhance drug bioavailability and provide precise control over drug release and activation at target sites.[44–46] SDT can also be used for spatiotemporally specific activation of immunotherapeutic prodrugs to alleviate irAEs.[47–49] Pu's group designed a nano-immunocomplex by covalently immobilizing PD-L1 antibody, adenosine deaminase (ADA) and a sonosensitizer into one entity with silenced activity.[47] Under sono-irradiation in the acidic TME, however, checkpoint blockade and immunometabolic reprogramming activities could be awakened as acid-cleavable and singlet oxygen-activatable linkers break. In our previous study, a prodrug nanopotentiator was constructed by cross-linking ADA with chlorin e6 (Ce6)-conjugated manganese dioxide nanoparticles *via* a ROS-cleavable linker.[48] The ADA was only activated after US irradiation to enhance the immune response initiated by SDT and chemodynamic therapy. However, the application of SDT using US-responsive prodrug nanomedicine to improve the efficacy and minimize the irAEs of immunotherapy against GBM has been poorly explored.

In the present study, an *in situ* sono-activatable prodrug hydrogel was designed to achieve precise sono-immunotherapy against GBM. Alginate (ALG) hydrogels were loaded with sonodynamic semiconducting polymer nanoparticles (SPNs) and the NLG919 prodrug to construct hydrogels (APN). The NLG919 prodrug was synthesized by conjugating monomethoxy polyethylene glycol (mPEG) with NLG919 using a singlet $^1O_2$-cleavable linker (mPEG-TK-NLG919, Fig. 1a). Poly [2,7-(9,9-di-octyl-fluorene)-*alt*-4,7-bis(thiophen-2-yl)benzo-2,1,3-thiadiazole] (PFODBT) was converted to water-soluble semiconducting polymer nanoparticles (SPNs) *via* nanoprecipitation with amphiphilic Pluronic F127. Such SPNs acted as sonosensitizers to generate $^1O_2$ upon exposure to US irradiation. After local injection of ALG solution containing SPNs and the NLG919 prodrug, the ALG hydrogels were *in situ* formed *via* coordination with Ca^{2+} in the TME. The sonodynamic effect of SPNs not only induced cell apoptosis and ICD of tumor cells, but also triggered active NLG919 release due to the specific breaking of $^1O_2$-cleavable linkers (Fig. 1b). As a result, the APN hydrogels synergistically integrated SDT with sono-activatable immunotherapeutic action to enable the deep-tissue combinational therapeutic effect for inhibiting tumor growth in an orthotopic glioma model.

2. Results and discussion

2.1. Preparation and characterization of prodrug hydrogels

To synthesize the $^1O_2$-responsive PEGylated NLG919 prodrug, mPEG-NH_2 was first reacted with an $^1O_2$-cleavable COOH-TK-COOH linker *via* an amide coupling reaction. The appearance of a peak at 1.5 ppm in ^1H NMR indicated the successful synthesis of mPEG-TK-COOH (Fig. S1, ESI†). Then, the carboxyl groups of the obtained mPEG-TK-COOH underwent an esterification reaction with the hydroxyl groups of NLG919 to produce mPEG-TK-NLG919, which was also characterized by ^1H NMR (Fig. S2, ESI†). Semiconducting polymer PFODBT was transformed into water-soluble polymeric nanoparticles *via* nanoprecipitation with amphiphilic Pluronic F127. The hydrodynamic diameter and zeta potential of the as-prepared nanoparticles were 52.7 nm (Fig. S3, ESI†) and −21.4 mV, respectively, indicating the successful self-assembly of SPNs. The characteristic UV-vis peaks of PFODBT were observed in SPNs and ALG solution containing SPNs (Fig. 2a). In addition, the fluorescence emission of PFODBT was similar in AP and APN solutions (Fig. 2b), suggesting that the loading of the NLG919 prodrug did not affect the optical properties of PFODBT.

The APN prodrug hydrogel was prepared by injecting ALG solution containing mPEG-TK-NLG919 and SPNs into Ca^{2+} solution (1.8 mM). The hydrogel was formed due to the cross-linking of Ca^{2+} and ALG. An ALG concentration of 5 mg mL^{-1} was selected because our previous studies have proved that this concentration could ensure quick gelation of hydrogels.[46,50]

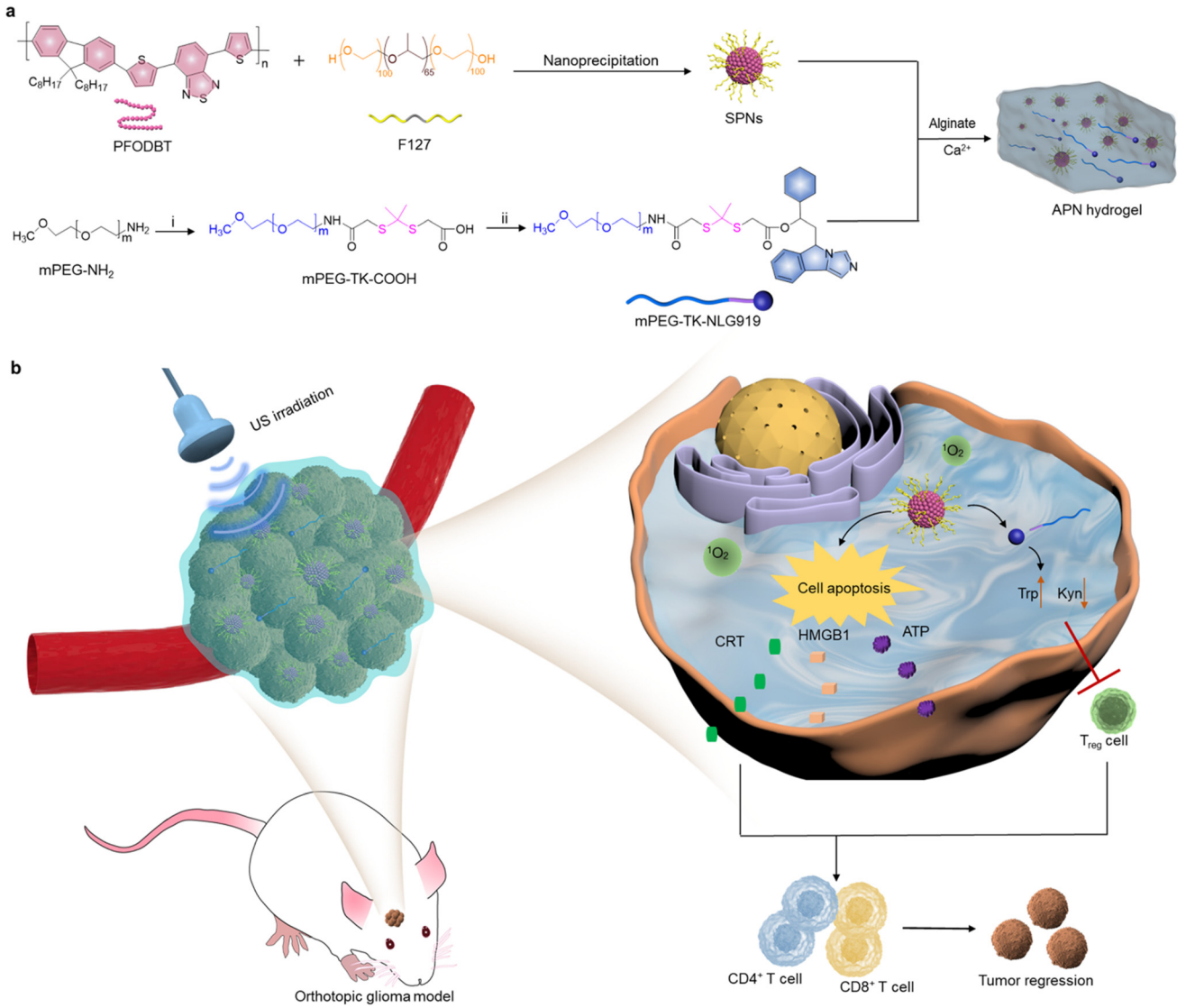

Fig. 1 Schematic illustration of the preparation and application of prodrug hydrogels in glioblastoma (GBM) sonodynamic immunotherapy. (a) The fabrication procedure of activatable prodrug hydrogels. (i): COOH-TK-COOH and EDC/NHS. (ii): EDC, DMAP, and NLG919. (b) Mechanism of prodrug hydrogel-mediated combinational sonodynamic therapy and immunotherapy for GBM.

The encapsulation efficiency and loading capacity of NLG919 in hydrogel APNs were calculated to be 86.2% and 1.0%, respectively. The hydrogel gelled rapidly in Ca^{2+} solution (1.8 mM) and the formed hydrogels remained stable after 24 h (Fig. 2c & S4†). The SEM images of the hydrogels showed cross-linked surface network structures and attached nanoparticles (Fig. 2d, Fig. S5, ESI†), similar to the control hydrogel without the NLG919 prodrug (Fig. S6, ESI†).

The $^1O_2$ generation efficiency of the prodrug hydrogel after US irradiation was evaluated using an $^1O_2$ indicator SOSG. The fluorescence intensity of SOSG was gradually increased after US irradiation for AP and APN hydrogels (Fig. S7, ESI†), indicating the generation of $^1O_2$. After 10 min of US irradiation, the SOSG fluorescence intensity at 528 nm was increased by 1.65- and 1.73-fold for AP and APN hydrogels (Fig. 2e). A similar increment of SOSG fluorescence intensity was observed in SPNs exposed to sono-irradiation (Fig. S8, ESI†). These results suggested that the formation of ALG-based hydrogels did not affect the $^1O_2$ generation efficiency of sonosensitizer SPNs.

As the TK linker could be destroyed by reactive oxygen species (ROS),[46] the mPEG-TK-NLG919 was postulated to be responsive to $^1O_2$. The release behavior of active NLG919 from the hydrogel was thus investigated. The release behavior of NLG919 from its prodrug form was monitored by HPLC after US irradiation for different times (Fig. S9†). Without US irradiation, the proportion of active NLG919 release from APN hydrogels remained around 30% after 15 min of incubation in aqueous solution. In contrast, nearly 80% of NLG919 was released from the prodrug hydrogel after 5 min of US irradiation and the cumulative release of active NLG919 could reach around 90% after 15 min of US irradiation (Fig. 2f).

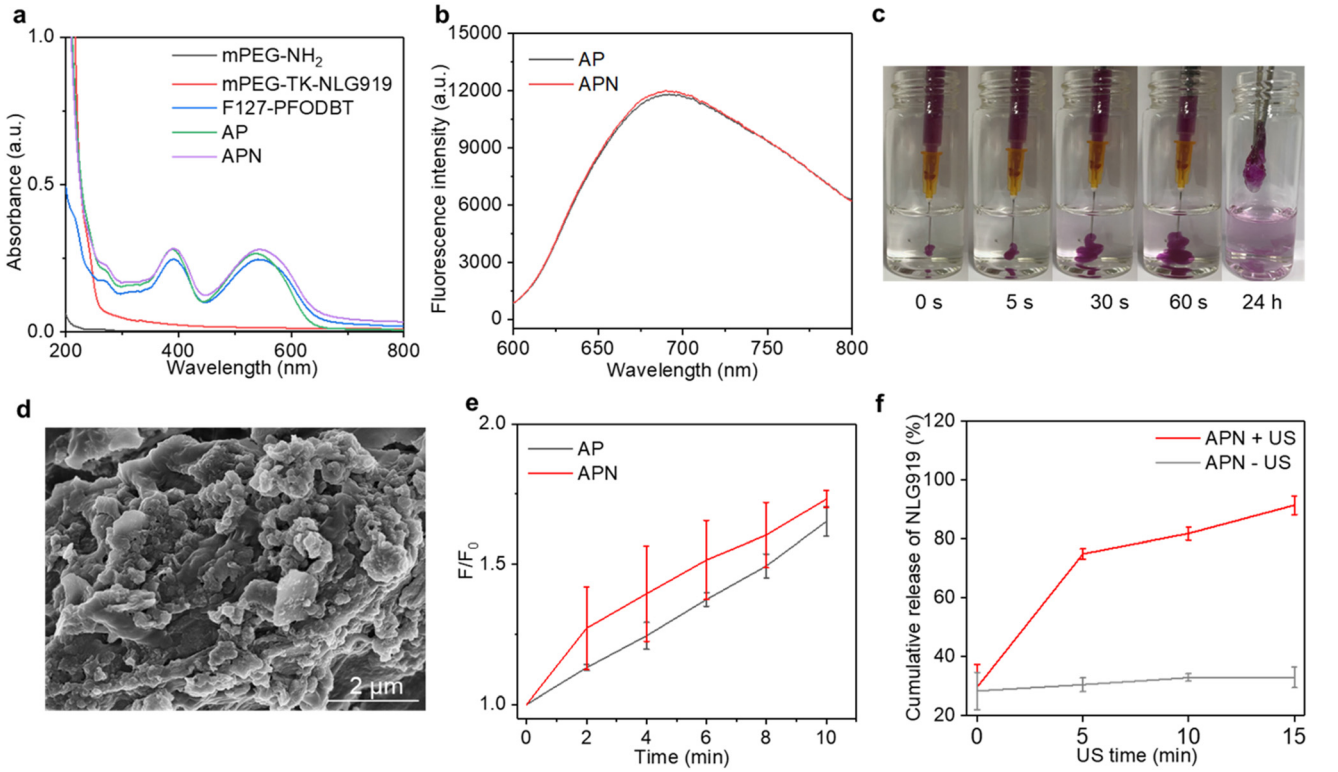

Fig. 2 Characterization of prodrug hydrogels. (a) UV-vis spectra of mPEG-NH_2, NLG919 prodrug (mPEG-TK-NLG919), SPNs, AP and APN in aqueous solution. (b) Fluorescence spectra of AP and APN hydrogels. (c) Gel formation process of APN hydrogels. (d) SEM images of APN hydrogels. (e) $^1O_2$ generation for AP and APN hydrogels as a function of ultrasound (US) irradiation time. (f) Cumulative release of NLG919 from the APN hydrogel after different times with or without US irradiation.

Therefore, the significant release of active NLG919 could be attributed to the $^1O_2$-mediated linker cleavage of the NLG prodrug upon US irradiation. In summary, these results indicated that the NLG919 prodrug could be activated and released from the loose structure of the hydrogel.

2.2. *In vitro* therapeutic efficacy of prodrug hydrogels and putative mechanisms

To evaluate the *in vitro* therapeutic efficacy of prodrug hydrogels, CCK-8 assay was used. The cytotoxicity of semiconducting polymer SPNs was first assessed. The cell viability of C6 cells remained approximately 90% even when the nanoparticle concentration was increased to 50 μg mL^{-1} (Fig. S10, ESI†), suggesting excellent biocompatibility of the as-prepared SPNs. The cell viability of AP and APN was also over 90% even when the concentration was increased to 50 μg mL^{-1}, suggesting that loading of nanoparticles into ALG hydrogel did not affect the biosafety of nanoparticles (Fig. 3a). The IC_{50} value was found to be 100.7 μg mL^{-1} and 102.5 μg mL^{-1} for AP and APN hydrogels, respectively (Fig. S11†). To explore the SDT effects on tumor cells, a DCFH-DA fluorescent probe was used to detect the generation of intracellular ROS under US irradiation. Although SOSG is a fluorescence sensor that detects $^1O_2$, it is a cell-impermeant probe and thus does not allow for intracellular $^1O_2$ detection.[51] Therefore, DCFH-DA served as a surrogate for SOSG in detecting intracellular $^1O_2$.[52] As shown in Fig. 3b, no significant fluorescent signals were found in the cells treated with AP or APN hydrogels without US irradiation, similar to that of the PBS control cells. In contrast, strong DCFH signals could be observed in the cells treated with AP or APN hydrogels and US irradiation, reflecting the intracellular production of ROS. Semi-quantitative analysis of DCFH signals showed that the intensity of the fluorescence signal was comparable between the AP + US and APN + US-treated cells, significantly higher than cells in other treatment groups (Fig. 3c). These results showed that both APN and AP hydrogels could robustly induce intracellular ROS production under US irradiation.

Encouraged by the remarkable ROS generation capacity of AP and APN hydrogels under US irradiation, the *in vitro* antitumor efficacy of these prodrug hydrogels on C6 glioma cells was investigated using the CCK-8 assay. In the absence of hydrogels, no obvious change in cell viability was observed in the sono-irradiated cells compared to the PBS control group (Fig. 3d). This indicated that the power and duration of US irradiation used here (1.0 W cm^{-2}, 2 min) did not cause observable damage to the cells. Nevertheless, cell viability was reduced to 6.68% and 5.07% after US irradiation for AP and APN hydrogel treatments, respectively. These results indicated that the hydrogel-mediated SDT upon US irradiation has a strong ability to kill cancer cells.

The damage to cancer cells by SDT has been reported to induce ICD in tumor cells.[39,40,53] When ICD occurs in tumor

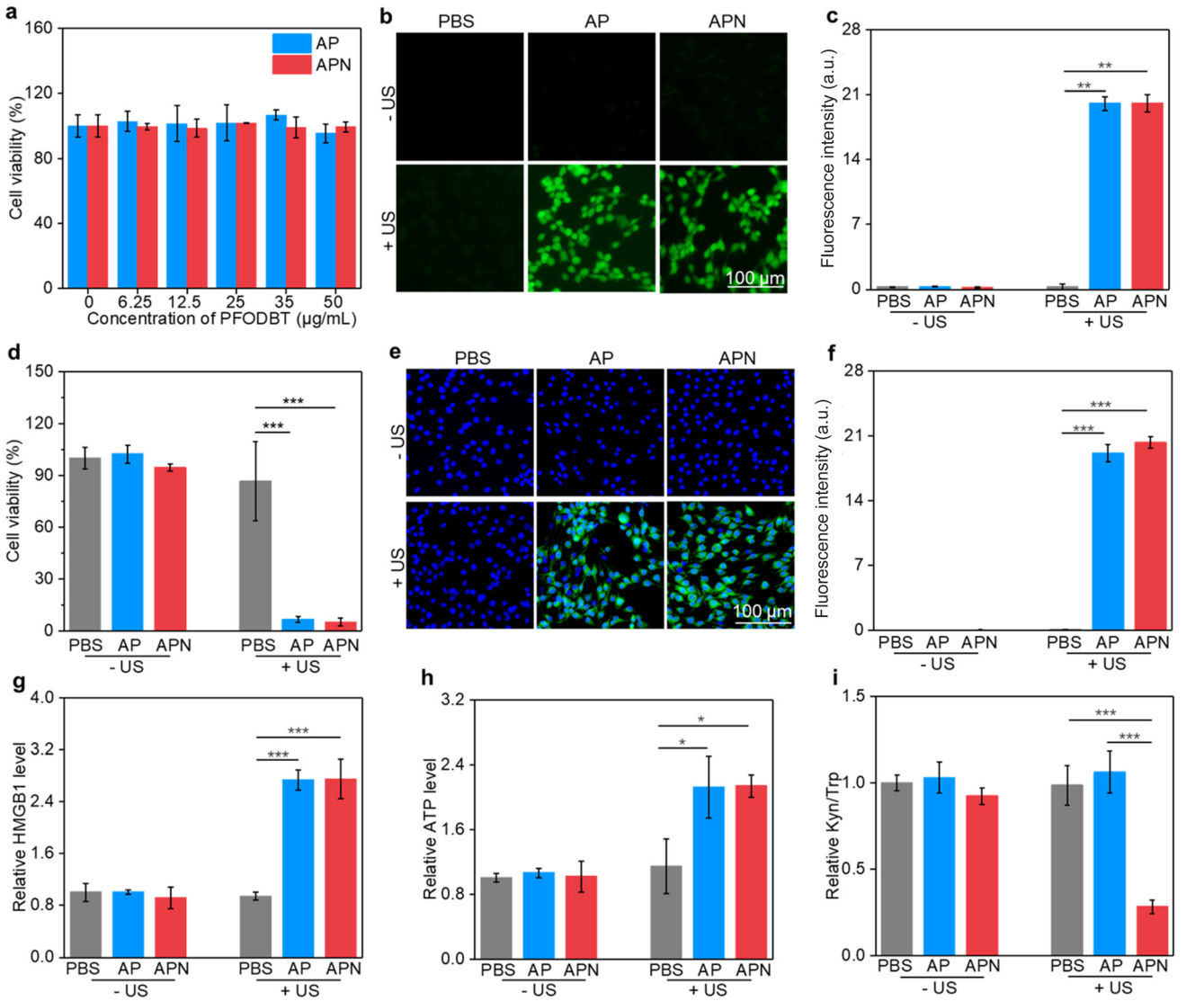

Fig. 3 *In vitro* evaluation of therapeutic efficacy and putative mechanisms. (a) Cell viability of C6 cells after AP and APN hydrogel treatment. (b) Fluorescent images of intracellular ROS by DCFH-DA staining. The generation of ROS was indicated by green fluorescence. (c) Semi-quantification of the DCFH fluorescence intensity. (d) Cell viability of C6 cells after PBS, AP, and APN hydrogel treatment with or without US irradiation. (e) CRT expression levels of C6 cells in different treatment groups; the green fluorescence signal indicates CRT expression. (f) Semi-quantification of CRT expression. (g) Relative levels of HMGB1 release from C6 cells in different treatment groups. (h) Relative levels of ATP release from C6 cells after different treatments. (i) Ratio of Kyn/Trp in the supernatant of C6 cells in different treatment groups. SPNs in AP and APN were set at a concentration of 25 μg mL^{-1} and US was applied at 1.0 W cm^{-2} for 2 min.

cells, a series of signaling molecules such as damage-associated molecular patterns (DAMPs) are produced, along with the exposure of CRT proteins on the surface of tumor cells, exocytosis of HMGB1 and the release of ATP.[54] The DAMPs released by this process are able to activate a series of cytological responses and boost the antitumor immunity.[55] To evaluate the ICD induction ability of hydrogel-mediated SDT, the levels of DAMPs after different treatments were analyzed. An immunofluorescence study showed that CRT staining can only be observed in cells treated with AP or APN hydrogels plus US irradiation (Fig. 3e). Semi-quantitative analysis showed that the mean fluorescence intensity of CRT was 19.1 and 23.3 for the AP + US and APN + US groups, significantly higher than those in the other treatment groups (Fig. 3f). Similarly, HMGB1 release from C6 cells in the AP + US and APN + US hydrogel groups was 2.7-fold higher relative to that in the PBS group (Fig. 3h). The ATP release was increased by around 2.2-fold when C6 cells were treated with AP or APN hydrogels followed by US irradiation (Fig. 3g). These results confirmed that the prodrug hydrogel-mediated SDT could robustly induce ICD, as demonstrated by the increased expression of CRT and the release of HMGB1 and ATP.

IDO is overexpressed in the TME and suppresses antitumor immunity *via* regulating Trp metabolism.[56] NLG919 is a specific IDO inhibitor with the ability to block Trp metabolism and promote antitumor immunity. To confirm the inhibitory

effect of the prodrug hydrogel on IDO activity and its intervention on Trp metabolism, the HPLC method was used to measure the concentrations of Trp and Kyn in the supernatants of the cell culture. The Kyn/Trp ratio did not show any significant differences from the control group in the APN hydrogel treatment group without US irradiation as well as in the AP group with US irradiation. In contrast, the application of APN hydrogels with US irradiation resulted in a significant decrease in the Kyn/Trp ratio of the cell culture supernatant, which was approximately 2.8-fold lower than that of the control group. These results supported the hypothesis that the sono-activation of the APN prodrug hydrogel could modulate Trp metabolism.

2.3. *In vivo* evaluation of antitumor efficacy and ICD induction

All animal experiments were performed in accordance with the Guidelines for the Care and Use of Laboratory Animals of Donghua University and approved by the Animal Ethics Committee of Donghua University. To evaluate the antitumor efficacy of prodrug hydrogels, an orthotopic glioma model in the right striatum was established. ALG solution loaded with SPNs with or without the NLG919 prodrug was locally injected to ensure adequate drug accumulation and therapeutic efficacy. 24 h after hydrogel administration, US irradiation (1.0 W cm^{-2}) was applied to the right side of the skull for 10 min. Brain tissue was extracted 7 days after treatment to evaluate the antitumor efficacy of prodrug hydrogel-mediated sonodynamic immunotherapy (Fig. 4a). H&E staining revealed that both PBS with US irradiation and AP or APN hydrogels did not show observable effects on glioma growth (Fig. 4b). Combining AP or APN hydrogels with US irradiation led to significant tumor cell necrosis, with the APN + US group exhibiting the most pronounced effect.

As demonstrated in cell studies, ICD could be induced effectively by the prodrug hydrogel-mediated SDT. To evaluate the ability of prodrug hydrogel treatment to induce ICD *in vivo*, intratumoral CRT and HMGB1 expression as well as ATP levels were measured. The ATP release in the AP + US and APN + US treatment groups was 19.3- and 23.7-fold higher than that of the PBS control group, respectively. In contrast, no significant change in ATP release was observed in the PBS + US, AP, and APN treatment groups as compared to that in the PBS control group (Fig. 4c). Immunofluorescence staining showed that the green fluorescence signal of CRT was significantly increased in the APN + US irradiated group compared to that in the PBS control group, AP or APN without US irradiation groups (Fig. 4d). The mean fluorescence intensity of CRT in the AP + US and APN + US groups was 23.2- and 27.8-fold higher than that in the PBS group, respectively (Fig. 4e). Correspondingly, the expression of tumor HMGB1 was significantly increased in the AP + US and APN + US treatment groups (Fig. 4f). Semiquantitative analysis revealed that the mean fluorescence intensity of HMGB1 was 10.3- and 11.6-fold higher in the AP + US and APN + US groups, respectively, compared to that in the PBS group (Fig. 4g). The above results collectively verified that US irradiation of hydrogels could induce ICD in tumor cells, especially for APN hydrogels.

2.4. Assessment of the *in vivo* immune response

The *in vivo* immune responses for sonodynamic immunotherapy were assessed by evaluating the populations of T cells in glioma-bearing brain slices. $CD8^+$ and $CD4^+$ T cells are the two main effector T cell populations in antitumor immunity.[57] Treatment with AP hydrogel and US irradiation significantly increased the $CD8^+$ fluorescence signal intensity, reaching 5.9-fold higher than that of the PBS control group, while sole AP hydrogel treatment did not activate $CD8^+$ proliferation (Fig. 5a & b). The $CD8^+$ fluorescence intensity was further increased in the APN + US irradiated group, reaching 10.3-fold higher relative to that of the PBS group, which could be attributed to the sono-activation of NLG919 to intervene in Trp metabolism. However, no significant enhancement of $CD8^+$ fluorescence in the APN alone group was observed. Correspondingly, the $CD4^+$ fluorescence intensity in tumors treated with AP hydrogel and US irradiation reached 10.5-fold higher than that of the PBS group (Fig. 5c & d). A more significant increase in $CD4^+$ fluorescence signal intensity was observed in the APN + US irradiated group compared to the AP + US irradiated group, reaching 19.3-fold higher relative to that in the PBS group. Tumor-associated $Foxp3^+$ T_{reg} are an essential type of immunosuppressive cell within the TME and play a key role in hindering the activation of T-cell-based immunity.[58] Therefore, the population of T_{reg} in tumors after different treatments was also evaluated. As expected, the fluorescence signal intensity of $Foxp3^+$ was significantly suppressed in tumors from the AP + US irradiated group, which was 2.2-fold lower than that of the PBS group (Fig. 5e & f). Loading of the NLG919 prodrug in hydrogel further decreased the T_{reg} population, which was 40.6-fold lower relative to that of the PBS group. Based on the above results, it could be reasonable to speculate that the *in vivo* antitumor immune response was successfully activated after treatment with APN hydrogels and US irradiation. The most likely explanation is that PFODBT was irradiated by US to produce ROS, which induced ICD of tumor cells and triggered the release of active NLG919 from its prodrug form and hydrogel, resulting in effector T cell activation and T_{reg} inhibition.

2.5. *In vivo* biosafety evaluation

Due to the formation of hydrogels *in situ*, the systemic toxicity of hydrogel-based drug delivery could be markedly minimized, especially in GBM treatments.[32,59] The body weight growth of mice showed no obvious difference among different treatments (Fig. S12, ESI†), suggesting satisfactory *in vivo* safety. To further validate the biosafety of the hydrogel, H&E staining was performed on other major organs (the heart, liver, spleen, lungs and kidneys) of the mice in the experimental and control groups. No discernible histological changes were found in the major organs of mice in the APN + US group (Fig. S13, ESI†), confirming that APN hydrogels and US irradiation do not cause observable damage to normal organs. Altogether, these results indicated that *in situ* prodrug hydro-

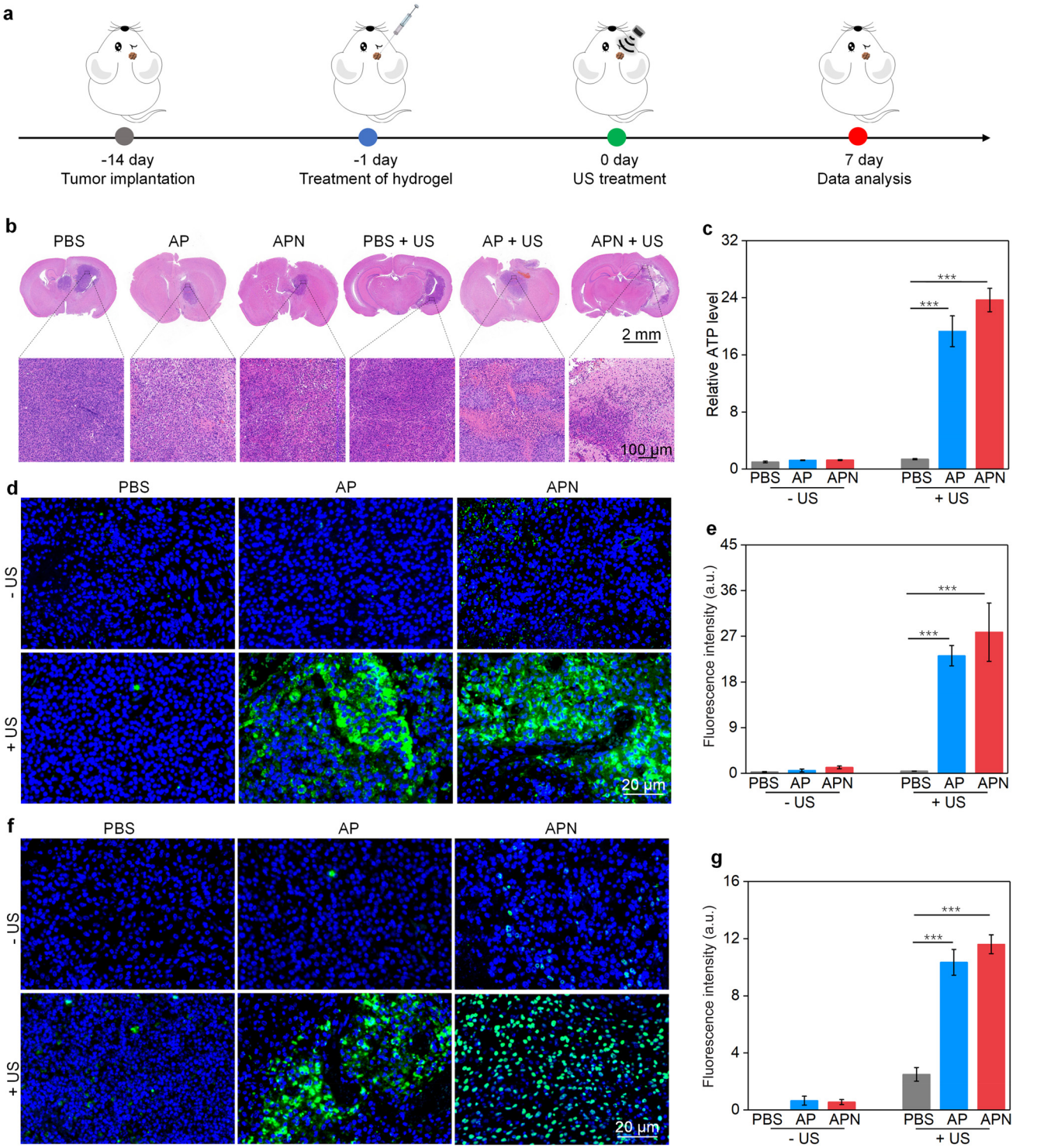

Fig. 4 *In vivo* antitumor efficacy and ICD induction evaluation. (a) Schematic diagram of antitumor efficacy evaluation by intracerebral implantation of C6 cancer cells, stereotactic injection of prodrug hydrogels and US irradiation (1.0 W cm^{-2}, 10 min). (b) H&E staining images of brain slices from glioma-bearing mice after different treatments. (c) Relative ATP release levels of tumor cells after different treatments. (d) Immunofluorescence CRT staining of tumors in different treatment groups. The green fluorescence signal indicates CRT and the blue signal indicates DAPI staining of the nucleus. (e) Semi-quantification of CRT expression. (f) Immunofluorescence staining images of HMGB1 in tumors after different treatments. The green fluorescence signal indicates HMGB1 staining while the blue fluorescence signal indicates DAPI staining of the nucleus. (g) Semi-quantification of the HMGB1 signal.

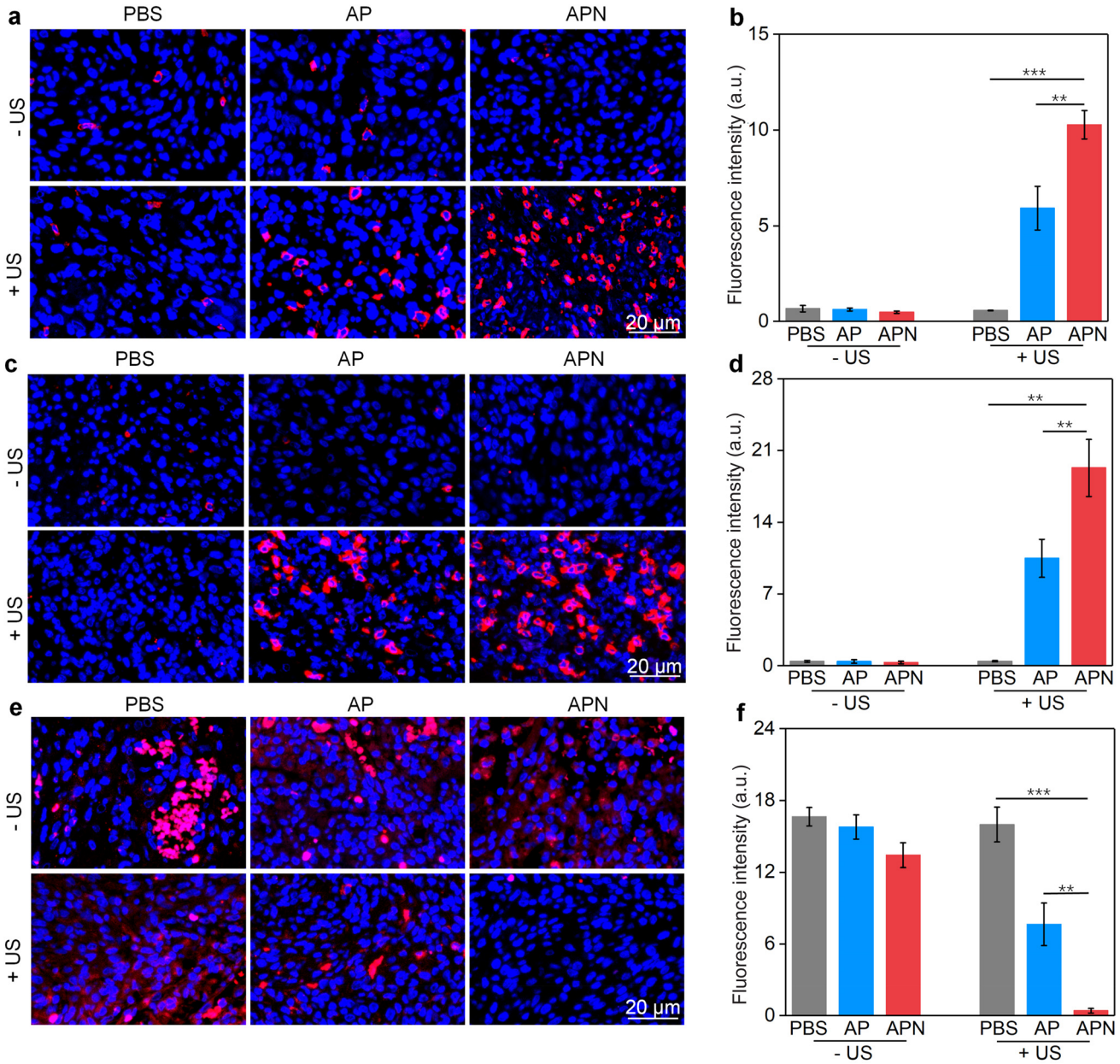

Fig. 5 *In vivo* immune response evaluation. (a) Immunofluorescence staining of CD8 in tumors from glioma-bearing mice after different treatments. Red fluorescence signals indicate CD8 staining and blue fluorescence signals indicate DAPI staining of the nucleus. (b) Semi-quantification of $CD8^+$ signals. (c) Immunofluorescence staining of CD4 in tumors. Red fluorescence signals indicate CD4 staining and blue fluorescence signals indicate DAPI staining of the nucleus. (d) Semi-quantification of $CD4^+$ signals. (e) Immunofluorescence staining of Foxp3 in tumors in different treatment groups. Red fluorescence signals indicate $Foxp3^+$ staining and blue fluorescence signals indicate DAPI staining of the nucleus. (f) Semi-quantification of $Foxp3^+$ signals.

gel-mediated sonodynamic immunotherapy could be a safe strategy for GBM treatment.

3. Conclusion

In summary, we report an US-responsive prodrug semiconducting polymer hydrogel platform for combined SDT and immunotherapy of orthotopic GBM. The hydrogel can be formed *in situ* at the tumor site and is loaded with SPNs for SDT and $^1O_2$-responsive prodrugs for immunotherapy. The SPNs produce $^1O_2$ after US irradiation to induce tumor cell necrosis and ICD. Meanwhile, the generated $^1O_2$ specifically destroy the responsive linker in the prodrug, allowing the on-demand release of the active IDO inhibitor NLG919, which potentiates antitumor immunity by inhibiting Trp metabolism to stimulate effector T cells and inhibit suppressive T_{reg}. Such a sono-responsive prodrug hydrogel showed a significant inhibitory

effect on the growth of orthotopic GBM. The efficacy and safety of GBM therapy were enhanced by the utility of prodrug hydrogels, which can be attributed to the inherent merits of a hydrogel platform, such as integrating different therapeutic approaches and allowing targeted drug release in the TME. To the best of our knowledge, APN hydrogel represents the first sono-activatable platform for combinational SDT and immunotherapy for GBM. Furthermore, the ease of the prodrug hydrogel preparation approach makes it possible to generalize it to load other drugs for GBM treatment.

Conflicts of interest

The authors declare no competing financial interest.

Acknowledgements

This work was financially supported by the Fundamental Research Funds for the Central Universities (2232021A-05), the Program for Professor of Special Appointment (Eastern Scholar) at Shanghai Institutions of Higher Learning, and the Science and Technology Commission of Shanghai Municipality (22490760700, 22ZR1401100, 20DZ2254900, and 22ZR1424900).

References

1 A. Omuro and L. M. DeAngelis, JAMA, Glioblastoma and other malignant gliomas: a clinical review, *J. Am. Med. Assoc.*, 2013, **310**(17), 1842–1850.
2 D. N. Louis, A. Perry, G. Reifenberger, A. von Deimling, D. Figarella-Branger, W. K. Cavenee, H. Ohgaki, O. D. Wiestler, P. Kleihues and D. W. Ellison, The 2016 world health organization classification of tumors of the central nervous system: a summary, *Acta Neuropathol.*, 2016, **23**(8), 1231–1251.
3 P. Y. Wen and D. A. Reardon, Neuro-oncology in 2015: Progress in glioma diagnosis, classification and treatment, *Nat. Rev. Neurol.*, 2016, **12**(2), 69–70.
4 A. C. Tan, D. M. Ashley, G. Y. Lopez, M. Malinzak, H. S. Friedman and M. Khasraw, Management of glioblastoma: State of the art and future directions, *Ca-Cancer J. Clin.*, 2020, **70**(4), 299–312.
5 L. R. Schaff and I. K. Mellinghoff, Glioblastoma and other primary brain malignancies in adults: A Review, *JAMA, J. Am. Med. Assoc.*, 2023, **329**(7), 574–587.
6 F. E. Bleeker, R. J. Molenaar and S. Leenstra, Recent advances in the molecular understanding of glioblastoma, *J. Neuro-Oncol.*, 2012, **108**, 11–27.
7 I. Mellman, G. Coukos and G. Dranoff, Cancer immunotherapy comes of age, *Nature*, 2011, **480**, 480–489.
8 J. Nam, S. Son, K. S. Park, W. Zou, L. D. Shea and J. J. Moon, Cancer nanomedicine for combination cancer immunotherapy, *Nat. Rev. Mater.*, 2019, **4**, 398–414.
9 N. Gong, N. C. Sheppard, M. M. Billingsley, C. H. June and M. J. Mitchell, Nanomaterials for T-cell cancer immunotherapy, *Nat. Nanotechnol.*, 2021, **16**, 25–36.
10 A. van Weverwijk and K. E. de Visser, Mechanisms driving the immunoregulatory function of cancer cells, *Nat. Rev. Cancer*, 2023, **23**(4), 193–215.
11 S. Xu, L. Tang, X. Li, F. Fan and Z. Liu, Immunotherapy for glioma: Current management and future application, *Cancer Lett.*, 2020, **476**, 1–12.
12 D. F. Quail and J. A. Joyce, The microenvironmental landscape of brain tumors, *Cancer Cell*, 2017, **31**(3), 326–341.
13 K. I. Woroniecka, K. E. Rhodin, P. Chongsathidkiet, K. A. Keith and P. E. Fecci, T-cell dysfunction in glioblastoma: Applying a new framework T-cell dysfunction in glioblastoma, *Clin. Cancer Res.*, 2018, **24**(16), 3792–3802.
14 M. Lim, Y. Xia, C. Bettegowda and M. Weller, Current state of immunotherapy for glioblastoma, *Nat. Rev. Clin. Oncol.*, 2018, **15**, 422–442.
15 C. M. Jackson, J. Choi and M. Lim, Mechanisms of immunotherapy resistance: lessons from glioblastoma, *Nat. Immunol.*, 2019, **20**, 1100–1109.
16 S. Zhou, Y. Huang, Y. Chen, Y. Liu, L. Xie, Y. You, S. Tong, J. Xu, G. Jiang, Q. Song, N. Mei, F. Ma, X. Gao, H. Chen and J. Chen, Reprogramming systemic and local immune function to empower immunotherapy against glioblastoma, *Nat. Commun.*, 2023, **14**(1), 435.
17 Y. Xu, J. Xiong, X. Sun and H. Gao, Targeted nanomedicines remodeling immunosuppressive tumor microenvironment for enhanced cancer immunotherapy, *Acta Pharm. Sin. B*, 2022, **12**(12), 4327–4347.
18 D. A. Wainwright, I. V. Balyasnikova, A. L. Chang, A. U. Ahmed, K. S. Moon, B. Auffinger, A. L. Tobias, Y. Han and M. S. Lesniak, IDO expression in brain tumors increases the recruitment of regulatory T cells and negatively impacts survival, *Clin. Cancer Res.*, 2012, **18**(22), 6110–6121.
19 O. Bloch, C. A. Crane, R. Kaur, M. Safaee, M. J. Rutkowski and A. T. Parsa, Gliomas promote immunosuppression through induction of B7-H1 expression in tumor-associated macrophages, *Clin. Cancer Res.*, 2013, **19**(12), 3165–3175.
20 M. P. Colombo and S. Piconese, Regulatory-T-cell inhibition versus depletion: the right choice in cancer immunotherapy, *Nat. Rev. Cancer*, 2007, **7**(11), 880–887.
21 J. H. Sampson, M. D. Gunn, P. E. Fecci and D. M. Ashley, Brain immunology and immunotherapy in brain tumours, *Nat. Rev. Cancer*, 2020, **20**, 12–25.
22 W. Tomaszewski, L. Sanchez-Perez, T. F. Gajewski and J. H. Sampson, Brain tumor microenvironment and host state: Implications for immunotherapy, *Clin. Cancer Res.*, 2019, **25**(14), 4202–4210.
23 A. Sabbagh, K. Beccaria, X. Ling, A. Marisetty, M. Ott, H. Caruso, E. Barton, L. Y. Kong, D. Fang, K. Latha, D. Y. Zhang, J. Wei, J. DeGroot, M. A. Curran, G. Rao, J. Hu, C. Desseaux, G. Bouchoux, M. Canney, A. Carpentier and A. B. Heimberger, Brain tumor microenvironment and host state: Implications for immunotherapy, eimberger, opening

of the blood-brain barrier using low-intensity pulsed ultrasound enhances responses to immunotherapy in preclinical glioma models, *Clin. Cancer Res.*, 2021, **27**(15), 4325–4337.

24 H. Wang, Y. Chao, H. Zhao, X. Zhou, F. Zhang, Z. Zhang, Z. Li, J. Pan, J. Wang, Q. Chen and Z. Liu, Smart nanomedicine to enable crossing blood-brain barrier delivery of checkpoint blockade antibody for immunotherapy of glioma, *ACS Nano*, 2022, **16**(1), 664–674.

25 K. J. Wolf, J. Chen, J. Coombes, M. K. Aghi and S. Kumar, Dissecting and rebuilding the glioblastoma microenvironment with engineered materials, *Nat. Rev. Mater.*, 2019, **4**, 651–668.

26 B. Decraene, Y. Yang, F. De Smet, A. D. Garg, P. Agostinis and S. De Vleeschouwer, Immunogenic cell death and its therapeutic or prognostic potential in high-grade glioma, *Genes Immun.*, 2022, **23**(8), 1–11.

27 T. Sun, Y. Li, Y. Yang, B. Liu, Y. Cao and W. Yang, Enhanced radiation-induced immunogenic cell death activates chimeric antigen receptor T cells by targeting CD39 against glioblastoma, *Cell Death Dis.*, 2022, **13**(10), 875.

28 B. Du and D. J. Waxman, Medium dose intermittent cyclophosphamide induces immunogenic cell death and cancer cell autonomous type I interferon production in glioma models, *Cancer Lett.*, 2020, **470**, 170–180.

29 L. Zhang, L. Xu, Y. Wang, J. Liu, G. Tan, F. Huang, N. He and Z. Lu, A novel therapeutic vaccine based on graphene oxide nanocomposite for tumor immunotherapy, *Chin. Chem. Lett.*, 2022, **33**(8), 4089–4095.

30 G. Catania, G. Rodella, K. Vanvarenberg and V. Preat, Combination of hyaluronic acid conjugates with immunogenic cell death inducer and CpG for glioblastoma local chemo-immunotherapy elicits an immune response and induces long-term survival, A. Malfanti, *Biomaterials*, 2023, **294**, 122006.

31 B. Abadi, N. Yazdanpanah, A. Nokhodchi and N. Rezaei, Smart biomaterials to enhance the efficiency of immunotherapy in glioblastoma: State of the art and future perspectives, *Adv. Drug Delivery Rev.*, 2021, **179**, 114035.

32 J. Zhang, C. Chen, A. Li, W. Jing, P. Sun, X. Huang, Y. Liu, S. Zhang, W. Du, R. Zhang, Y. Liu, A. Gong, J. Wu and X. Jiang, Immunostimulant hydrogel for the inhibition of malignant glioma relapse post-resection, *Nat. Nanotechnol.*, 2021, **16**(5), 538–548.

33 Z. Dai, J. Tang, Z. Gu, Y. Wang, Y. Yang, Y. Yang and C. Yu, Eliciting immunogenic cell death via a unitized nanoinducer, *Nano Lett.*, 2020, **20**(9), 6246–6254.

34 M. Trendowski, The promise of sonodynamic therapy, *Cancer Metastasis Rev.*, 2014, **33**, 143–160.

35 Y. Yin, X. Jiang, L. Sun, H. Li, C. Su, Y. Zhang, G. Xu, X. Li, C. Zhao and Y. Chen, Continuous inertial cavitation evokes massive ROS for reinforcing sonodynamic therapy and immunogenic cell death against breast carcinoma, *Nano Today*, 2021, **36**, 101009.

36 X. Wang, X. Wang, Q. Yue, H. Xu, X. Zhong, L. Sun, G. Li, Y. Gong, N. Yang and Z. Wang, Liquid exfoliation of TiN nanodots as novel sonosensitizers for photothermal-enhanced sonodynamic therapy against cancer, *Nano Today*, 2021, **39**, 101170.

37 X. Qian, Y. Zheng and Y. Chen, Micro/nanoparticle-augmented sonodynamic therapy (SDT): breaking the depth shallow of photoactivation, *Adv. Mater.*, 2016, **28**(37), 8097–8129.

38 F. Jiang, C. Yang, B. Ding, S. Liang, Y. Zhao, Z. Cheng, M. Liu, B. Xing, P. Ma and J. Lin, Tumor microenvironment-responsive $MnSiO_3$-Pt@BSA-Ce6 nanoplatform for synergistic catalysis-enhanced sonodynamic and chemodynamic cancer therapy, *Chin. Chem. Lett.*, 2022, **33**(6), 2959–2964.

39 Y. Si, J. Yue, Z. Liu, M. Li, F. Du, X. Wang, Z. Dai, N. Hu, J. Ju, S. Gao, X. Wang and P. Yuan, Phase-transformation nanoparticle-mediated sonodynamic therapy: An effective modality to enhance anti-tumor immune response by inducing immunogenic cell death in breast cancer, *Int. J. Nanomed.*, 2021, **16**, 1913–1926.

40 S. Liang, J. Yao, D. Liu, L. Rao, X. Chen and Z. Wang, Harnessing nanomaterials for cancer sonodynamic immunotherapy, *Adv. Mater.*, 2023, e2211130.

41 R. S. Riley, C. H. June, R. Langer and M. J. Mitchell, Delivery technologies for cancer immunotherapy, *Nat. Rev. Drug Discovery*, 2019, **18**(3), 175–196.

42 A. Xie, S. Hanif, J. Ouyang, Z. Tang, N. Kong, N. Y. Kim, B. Qi, D. Patel, B. Shi and W. Tao, Stimuli-responsive prodrug-based cancer nanomedicine, *EBioMedicine*, 2020, **56**, 102821.

43 B. Yang, J. Gao, Q. Pei, H. Xu and H. Yu, Engineering prodrug nanomedicine for cancer immunotherapy, *Adv. Sci.*, 2020, **7**(23), 2002365.

44 S. Zhou, X. Hu, R. Xia, S. Liu, Q. Pei, G. Chen, Z. Xie and X. Jing, A paclitaxel prodrug activatable by irradiation in a hypoxic microenvironment, *Angew. Chem., Int. Ed.*, 2020, **59**(51), 23198–23205.

45 S. Li, X. Shan, Y. Wang, Q. Chen, J. Sun, Z. He, B. Sun and C. Luo, Dimeric prodrug-based nanomedicines for cancer therapy, *J. Controlled Release*, 2020, **326**, 510–522.

46 M. Ding, Y. Fan, Y. Lv, J. Liu, N. Yu, D. Kong, H. Sun and J. Li, A prodrug hydrogel with tumor microenvironment and near-infrared light dual-responsive action for synergistic cancer immunotherapy, *Acta Biomater.*, 2022, **149**, 334–346.

47 C. Zhang, J. Huang, Z. Zeng, S. He, P. Cheng, J. Li and K. Pu, Catalytical nano-immunocomplexes for remote-controlled sono-metabolic checkpoint trimodal cancer therapy, *Nat. Commun.*, 2022, **13**(1), 3468.

48 M. Zhan, F. Wang, Y. Liu, J. Zhou, W. Zhao, L. Lu, J. Li and X. He, Dual-cascade activatable nanopotentiators reshaping adenosine metabolism for sono-chemodynamic-immunotherapy of deep tumors, *Adv. Sci.*, 2023, 2207200.

49 J. Li, Y. Luo, Z. Zeng, D. Cui, J. Huang, C. Xu, L. Li, K. Pu and R. Zhang, Precision cancer sono-immunotherapy using deep-tissue activatable semiconducting polymer immunomodulatory nanoparticles, *Nat. Commun.*, 2022, **13**(1), 4032.

50 J. Liu, X. Qing, Q. Zhang, N. Yu, M. Ding, Z. Li, Z. Zhao, Z. Zhou and J. Li, Oxygen-producing proenzyme hydrogels for photodynamic-mediated metastasis-inhibiting combinational therapy, *J. Mater. Chem. B*, 2021, **9**(26), 5255–5263.
51 W. Hou, Y. Yuan, Z. Sun, S. Guo, H. Dong and C. Wu, Ratiometric fluorescent detection of intracellular singlet oxygen by semiconducting polymer dots, *J. Anal. Chem.*, 2018, **90**(24), 14629–14634.
52 J. Fu, T. Li, Y. Zhu and Y. Hao, Ultrasound-activated oxygen and ROS generation nanosystem systematically modulates tumor microenvironment and sensitizes sonodynamic therapy for hypoxic solid tumors, *Adv. Funct. Mater.*, 2019, **29**(51), 1906195.
53 H. Chen, L. Liu, A. Ma, T. Yin, Z. Chen, R. Liang, Y. Qiu, M. Zheng and L. Cai, Noninvasively immunogenic sonodynamic therapy with manganese protoporphyrin liposomes against triple-negative breast cancer, *Biomaterials*, 2021, **269**, 120639.
54 D. V. Krysko, A. D. Garg, A. Kaczmarek, O. Krysko, P. Agostinis and P. Vandenabeele, Immunogenic cell death and DAMPs in cancer therapy, *Nat. Rev. Cancer*, 2012, **12**(12), 860–875.
55 Z. Li, X. Lai, S. Fu, L. Ren, H. Cai, H. Zhang, Z. Gu, X. Ma and K. Luo, Immunogenic cell death activates the tumor immune microenvironment to boost the immunotherapy efficiency, *Adv. Sci.*, 2022, **9**(22), 2201734.
56 Y. W. Moon, J. Hajjar, P. Hwu and A. Naing, Targeting the indoleamine 2,3-dioxygenase pathway in cancer, *J. Immunother. Cancer*, 2015, **3**, 51.
57 M. Z. Madden and J. C. Rathmell, The complex integration of T-cell metabolism and immunotherapy, *Cancer Discovery*, 2021, **11**(7), 1636–1643.
58 C. Tay, A. Tanaka and S. Sakaguchi, Tumor-infiltrating regulatory T cells as targets of cancer immunotherapy, *Cancer Cell*, 2023, **41**(3), 450–465.
59 X. Wang, L. Ye, W. He, C. Teng, S. Sun, H. Lu, S. Li, L. Lv, X. Cao, H. Yin, W. Lv and H. Xin, In situ targeting nanoparticles-hydrogel hybrid system for combined chemo-immunotherapy of glioma, *J. Controlled Release*, 2022, **345**, 786–797.